PERGAMON

International Journal of Solids and Structures 40 (2003) 3293–3310

INTERNATIONAL JOURNAL OF SOLIDS and STRUCTURES

www.elsevier.com/locate/ijsolstr

On Saint-Venant's principle in the dynamics of elastic beams

V. Berdichevsky, D.J. Foster *

Department of Mechanical Engineering, Wayne State University, Detroit, MI 48202, USA

Received 22 August 2002; received in revised form 4 January 2003

Abstract

In dynamics, Saint-Venant's principle of exponential decay of stress resulting from a self-equilibrating load is not valid. For a beam type structure, a self-equilibrated load may penetrate well inside the beam. Although this effect has been known for a long time, at least since Lamb's paper [Proc. Roy. Soc. Lon. Ser. A 93 (1916) 114], it was not clear how to characterize it quantitatively. In this paper we propose a ''probabilistic approach'' to evaluate the magnitude of the penetrating stress state. The key point is that, in engineering problems, the distribution of the self-equilibrated load is usually not known. By assigning to the self-equilibrated load some probabilistic measure one can find probabilistic characteristics of the penetrating stress state. We develop this reasoning for the simplest case: longitudinal vibrations of a two-dimensional semi-infinite, elastic isotropic homogeneous strip, excited by a periodic load at the end. We show the frequency range where Saint-Venant's principle can be used with good accuracy, and thus, one-dimensional classical beam theory still can be applied. We characterize also the increase in this range which is achieved in the refined plate theory proposed by Berdichevsky and Le [J. Appl. Math. Mech. (PMM) 42 (1) (1978) 140].

1. Introduction

Consider a semi-infinite elastic beam, a cylindrical elastic body of arbitrary cross-section, as shown in Fig. 1. The x-axis is directed along the beam, and axes x_1, x_2 are in the beam cross-section A, $(x_1, x_2) \in A$; $0 \leqslant x \leqslant \infty$. Let the lateral surface of the beam be free of load. At the left end, $x = 0$, some forces $\boldsymbol{p} = (p_1, p_2, p)$ are applied. De Saint-Venant (1885) claimed that, in the case of static load, if the load is self-equilibrated, i.e. the total force and resultant moment are zero,

$$\int_A p_1 \, \mathrm{d}A = 0, \quad \int_A p_2 \, \mathrm{d}A = 0, \quad \int_A p \, \mathrm{d}A = 0 \tag{1.1}$$

$$\int_A p x_1 \, \mathrm{d}A = 0, \quad \int_A p x_2 \, \mathrm{d}A = 0, \quad \int_A (p_1 x_2 - p_2 x_1) \, \mathrm{d}A = 0 \tag{1.2}$$

* Corresponding author.
E-mail addresses: vberd@wayne.edu (V. Berdichevsky), dinver32@hotmail.com (D.J. Foster).

0020-7683/03/$ - see front matter © 2003 Elsevier Science Ltd. All rights reserved.
doi:10.1016/S0020-7683(03)00158-6

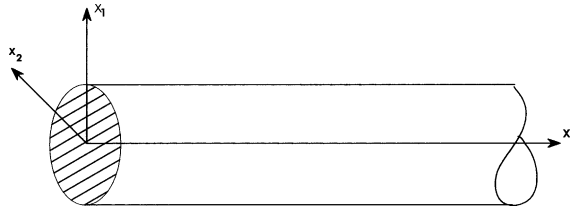

Fig. 1. Coordinate diagram.

then the stress decays fast in the x-direction. This statement is called Saint-Venant's principle. Neglecting the stress field caused by the self-equilibrating load reduces the study of the stress state away from the end to just the study of a two-dimensional elasticity problem on the cross-section A. In more complex cases, when the forces on the lateral surfaces are not zero, the general three-dimensional elasticity problem away from the ends can be split into a two-dimensional problem on the cross-section A and a one-dimensional problem along the beam—the so-called one-dimensional beam theory. Such splitting was presented in an inexplicit form already in Saint-Venant's memoir. It was recognized later that the splitting has an asymptotic nature: it is possible if the characteristic length of the changes of stresses along the beam is much bigger than the characteristic size of the cross section. Many papers contributed to studying various aspects of the splitting. In the case of general anisotropy and inhomogenuity the splitting was constructed by Berdichevsky (1981).

The first mathematical proof of Saint-Venant's principle was given by Toupin (1965). He showed that the stresses, σ, decay exponentially with distance from the loaded end, x as

$$\sigma = \sigma_0 \mathrm{e}^{-\gamma x} \tag{1.3}$$

The decay rate, γ, has the form

$$\gamma = \gamma_0/h \tag{1.4}$$

where h is a characteristic cross-section dimension and the dimensionless constant γ_0 depends only on the cross-section geometry and the elastic moduli. For beams with a full cross-section γ_0 is of the order of unity, and the stresses caused by the self-equilibrating load are localized at the vicinity of the beam end, and form a "boundary layer". There are cross-sectional geometries and inhomogeneous distributions of elastic moduli for which γ_0 becomes very small. In such cases one says that Saint-Venant's principle is violated. Due to (1.3) and (1.4), for γ_0 of the order of unity, the two-dimensional elasticity problems in the cross-section predict the true state of stress in the beam with exponentially small errors, in the order of $\exp(-\gamma_0 L/h)$, where L is the beam length. Toupin's paper (1965) initiated an explosion of studies on this subject. We note here Knowles (1966), Knowles and Horgan (1969), Horgan (1974), Berdichevsky (1974, 1976, 1978, 1981), Flavin and Knops (1987, 1988), Flavin et al. (1989), Vafeades and Horgan (1988), Flavin and Rionero (1993), the review by Horgan and Knowles (1983), and the review updates (Horgan, 1989, 1996). More recent papers have concentrated on situations where the decay rate is slow, as in orthotropic material by Matemilola and Stronge (1995); in laminated composite structures by Wijeyewickrema et al. (1996), Baxter and Horgan (1997), Tullini and Horgan (1998); and in thin wall beams Volovoi et al. (1999). Some related mathematical issues have been discussed by Mielke (1989) and Druz and Ustinov (1996). Nowadays a complete understanding of the matter has been developed.

The situation in dynamics is much more complex. We will focus here only on the case when the loading is periodic in time, and do not touch on the related case of impact loading that has been discussed by Novozhilov and Slepian (1964), Folk and Herczynski (1986), and Rassoulova (2001). The qualitative un-

derstanding of the situation became possible after Lamb's paper (1916), where all running wave solutions were obtained for the special case of the elastic isotropic homogeneous strip with stress free boundary.

Running wave solutions posses the following key features, which apply in the general three-dimensional case. At a given frequency ω there are an infinite number of running wave solutions of the form $ue^{i(kx-\omega t)}$, where u is a function of the cross-section coordinates. Each solution is characterized by the value of the wave number k. We will call them modes and also branches. The wave numbers k are the solutions of the dispersion equation $f(\omega, k) = 0$. The wave number k is, in general complex. The real-valued k correspond to penetrating modes, the complex-valued k to decaying or growing modes. For each ω, if there is a solution with some value of k, there are also solutions corresponding to $-k$, $\bar{k}$ and $-\bar{k}$ (the bar denotes complex conjugate).

Consider first the static case, $\omega = 0$. For $\omega = 0$ there is a multiple root of the dispersion equation $k = 0$; all non-zero roots are complex. In the three-dimensional case, the multiplicity of the root $k = 0$ is six. The corresponding modes are six independent rigid motions of the beam. The solution for an arbitrary loaded beam can be sought in the form of a sum of the mode solutions multiplied by arbitrary coefficients. The coefficients must be found from the boundary conditions at $x = 0$. One has to include in the sum only modes with $\mathrm{Im}\, k \geqslant 0$ to provide a solution bounded at infinity. Modes with non-zero k possess a remarkable property: they are all orthogonal (in energy) to the modes with zero k. This is why imposing six conditions (1.1) and (1.2) eliminates six non-decaying modes corresponding with $k = 0$: other modes drop out as orthogonal to the rigid cross-sectional motions. The situation changes for non-zero frequency ω. A qualitative dispersion picture is shown, for small ω in Fig. 2. Six branches appear out of the root $k = 0$, and a branch from each complex root. The six branches correspond to low frequency, long wave vibrations of elastic beams. They are described by classical one-dimensional beam theory. Four of the six branches have real values of k, two branches grow linearly with k and two grow quadratically with k. The linearly growing branches correspond to longitudinal and torsional vibrations; the quadratically growing branches correspond to flexural vibrations. Branches with real negative k correspond to the waves moving from right to left in Fig. 1. We do not consider cases with a source of stress at infinity, thus we do not take these branches into account subsequently. The remaining two of the six branches have pure imaginary k, and also involve flexural motions. Though vibrations corresponding to these two branches decay, the decay rate is very small at low frequency since the branches started from $k = 0$. For brevity, we will call all six branches penetrating modes. Along with these penetrating modes, there are branches with complex values of k. Those with positive imaginary parts are decaying in amplitude with increase in distance from the beam end.

More detailed pictures of dispersion curves can be found; see for example, Mindlin and Medick (1959), Mason (1964), Gregory and Gladwell (1983), Folk and Herczynski (1986), Meleshko and Tatuyan (1987), Volovoi et al. (1998), Pagneux and Maurel (2001) and the monograph by Le (1999).

A difficulty in the formulation of a dynamical version of Saint-Venant's principle is that the modes with complex k are no longer orthogonal to the penetrating modes. It is not clear how to formulate the conditions that eliminate the penetrating modes. Moreover, as will be seen from what follows, the conditions

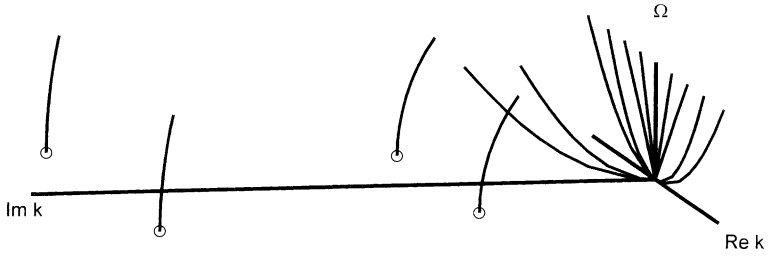

Fig. 2. Qualitative form of dispersion curves for low frequencies.

(1.1) and (1.2) do not prevent the generation of the penetrating modes, or, in other words, a self-equilibrated dynamic load may cause a penetrating stress state. An unpleasant consequence is that, in general, one cannot trust the predictions of dynamical one-dimension beam theory that takes into account only the total force and moment at the beam end.

This paper proposes a quantitative measure for the violation of Saint-Venant's Principle in dynamics. We use that the self-equilibrated part of the end load is not usually known in engineering problems. Therefore we treat the load as random, accept a probabilistic model for randomness and determine the probabilistic characteristics of the penetrating stress state. It is worth emphasizing that the actual load is not random, and that randomness only comes into play to model our absence of knowledge of the actual self-equilibrated part of the load. One may say that the information on the self-equilibrated part of the load is given in probabilistic terms, as a measure on the space of loads.

To simplify the technical details we focus on the simplest of dynamic problems: excitation of a semi-infinite elastic isotropic homogeneous strip by harmonic forces applied at the end. We obtain the standard deviation of the penetrating stress state from zero as a function of frequency ω. This allows us to characterize the frequency range for validity of classical beam theory in the problem under consideration. We evaluate also an expansion of this range achieved in the refined plate theory offered by Berdichevsky and Le (1980).

The material is organized as follows. In the next three sections we describe an extension of the Lamb solution for the semi-infinite strip. In Section 5 the probabilistic model is introduced, the method of determining the penetrating stress state outlined and results for symmetric loading presented. The conclusions drawn from the study are summarized in Section 6.

2. Vibrations of a semi-infinite strip

Consider a semi-infinite strip of homogeneous isotropic material with Lame elastic constants λ and μ and density ρ. It occupies the region $x \geqslant 0$, $-h \leqslant y \leqslant h$, unbounded in the z direction. The faces $y = h$ and $y = -h$ are free of traction, the end $x = 0$ is subjected to a load which changes harmonically with time t at a frequency ω. The load causes normal stresses σ_{xx} and σ_{yy} and shear stresses σ_{xy} with displacements u and v in the (x, y)-plane. The dynamic behavior is governed by the following equations:

The momentum equations,

$$\begin{aligned} &\frac{\partial \sigma_{xx}}{\partial x} + \frac{\partial \sigma_{xy}}{\partial y} - \rho \frac{\partial^2 u}{\partial t^2} = 0 \\ &\frac{\partial \sigma_{xy}}{\partial x} + \frac{\partial \sigma_{yy}}{\partial y} - \rho \frac{\partial^2 v}{\partial t^2} = 0 \end{aligned} \tag{2.1}$$

the stress–strain relations,

$$\begin{aligned} \sigma_{xx} &= \lambda\left(\frac{\partial u}{\partial x} + \frac{\partial v}{\partial y}\right) + 2\mu \frac{\partial u}{\partial x} \\ \sigma_{yy} &= \lambda\left(\frac{\partial u}{\partial x} + \frac{\partial v}{\partial y}\right) + 2\mu \frac{\partial v}{\partial y} \\ \sigma_{xy} &= \mu\left(\frac{\partial v}{\partial x} + \frac{\partial u}{\partial y}\right) \end{aligned} \tag{2.2}$$

the free boundary conditions at the faces of the strip

$$\sigma_{yy} = 0, \quad \sigma_{xy} = 0 \quad \text{at } y = \pm h \tag{2.3}$$

and the boundary conditions at the strip edge

$$\sigma_{xx}(y,t) = f_{xx}(y)\cos(\omega t) + g_{xx}(y)\sin(\omega t) \tag{2.4}$$

$$\sigma_{xy}(y,t) = f_{xy}(y)\cos(\omega t) + g_{xy}(y)\sin(\omega t) \tag{2.5}$$

The functions $f_{xx}(y)$, $f_{xy}(y)$, $g_{xx}(y)$ and $g_{xy}(y)$ are assumed to be given. There is also a condition that there are no forces at infinity, which we formulate explicitly later. It is easy to check that any solution of (2.1) and (2.2) can be presented as a sum of two solutions: a symmetric solution with $u(x,y,t)$, $\sigma_{xx}(x,y,t)$ and $\sigma_{yy}(x,y,t)$ even in y and $v(x,y,t)$ and $\sigma_{xy}(x,y,t)$ odd in y, and an antisymmetric solution having $v(x,y,t)$ and $\sigma_{xy}(x,y,t)$ even in y with $u(x,y,t)$, $\sigma_{xx}(x,y,t)$ and $\sigma_{yy}(x,y,t)$ odd in y. Symmetric solutions correspond to longitudinal vibrations, antisymmetric solutions to flexural vibrations. In this paper we will discuss only dynamic loads causing purely longitudinal vibrations. In this case, $f_{xx}(y)$ and $g_{xx}(y)$ are even functions of y while $f_{xy}(y)$ and $g_{xy}(y)$ are odd functions.

Following Lamb (1916), we seek such solutions of (2.1) and (2.2) that each unknown function has the form of a function of y multiplied by $e^{i(kx-\omega t)}$. It is convenient to write the equations in dimensionless form by introducing dimensionless stresses σ'_{xx}, σ'_{yy} and σ'_{xy}, coordinates x', y' and displacements u', v' by the relations

$$\sigma'_{xx} = \frac{\sigma_{xx}}{\mu}, \quad \sigma'_{yy} = \frac{\sigma_{yy}}{\mu}, \quad \sigma'_{xy} = \frac{\sigma_{xy}}{\mu}, \quad x' = \frac{x}{h}, \quad y' = \frac{y}{h}, \quad u' = \frac{u}{h}, \quad v' = \frac{v}{h} \tag{2.6}$$

Accordingly dimensionless quantities frequency Ω, time t' and wave number k' are defined as

$$\Omega^2 = \frac{\rho h^2 \omega^2}{\mu}, \quad t' = \frac{t}{h}\sqrt{\frac{\mu}{\rho}} \quad \text{and} \quad k' = kh \tag{2.7}$$

In what follows we omit the primes. Eqs. (2.1) and (2.2) take the form:

$$\begin{aligned} &ik\sigma_{xx} + \frac{\partial \sigma_{xy}}{\partial y} + \Omega^2 u = 0 \\ &ik\sigma_{xy} + \frac{\partial \sigma_{yy}}{\partial y} + \Omega^2 v = 0 \end{aligned} \tag{2.8}$$

$$\begin{aligned} \sigma_{xx} &= \frac{\lambda}{\mu}\left(iku + \frac{\partial v}{\partial y}\right) + 2iku \\ \sigma_{yy} &= \frac{\lambda}{\mu}\left(iku + \frac{\partial v}{\partial y}\right) + 2\frac{\partial v}{\partial y} \\ \sigma_{xy} &= ikv + \frac{\partial u}{\partial y} \end{aligned} \tag{2.9}$$

Eqs. (2.8) and (2.9) with free boundary conditions (2.3) determine an eigenvalue problem for the parameter k, dependent on the assigned frequency Ω. The corresponding operator is not self-adjoint, thus k is complex while the eigenfunctions are not orthogonal. The latter causes all the difficulties in establishing the extension of Saint-Venant's principle to dynamic loading.

Substitution from the three stress equations (2.9), into the momentum equations (2.8) yields two equations in terms of the displacements only:

$$\begin{aligned} &\mathrm{i}\frac{k}{1-2v}\frac{\partial v}{\partial y}+\left(\Omega^2-2\frac{1-v}{1-2v}k^2+\frac{\partial^2}{\partial y^2}\right)u=0\\ &\left(\Omega^2-k^2+2\frac{1-v}{1-2v}\frac{\partial^2}{\partial y^2}\right)v+\mathrm{i}\frac{k}{1-2v}\frac{\partial u}{\partial y}=0 \end{aligned} \tag{2.10}$$

where $v=(\lambda/2(\lambda+\mu))$ is Poisson's ratio. This is a system of two ordinary differential equations with constant coefficients. Thus a generic form for the solution is

$$u=u_0\mathrm{e}^{\alpha y},\quad v=v_0\mathrm{e}^{\alpha y} \tag{2.11}$$

with u_0, v_0 being some constants.

Substituting (2.11) in Eqs. (2.10), we obtain the system of two linear equations with respect to u_0, v_0:

$$\begin{bmatrix} \Omega^2-2\frac{1-v}{1-2v}k^2+\alpha^2 & \mathrm{i}\frac{k}{1-2v}\\ \mathrm{i}\frac{k}{1-2v} & \Omega^2-k^2+2\frac{1-v}{1-2v}\alpha^2 \end{bmatrix}\cdot\begin{bmatrix} u_0\\ v_0 \end{bmatrix}=0 \tag{2.12}$$

For a non-trivial solution, the determinant of the coefficient matrix in (2.12) must be zero. The determinant can be presented in the form

$$(k^2-\alpha^2-\Omega^2)\left(k^2-\alpha^2-\frac{1-2v}{(2-2v)}\Omega^2\right)=0 \tag{2.13}$$

We see that there are four possible values of α which depend on k and Ω. We denote one pair of the roots by $\pm\alpha$ and the second pair by $\pm\beta$,

$$\alpha^2=k^2-\frac{1-2v}{2-2v}\Omega^2,\quad \beta^2=k^2-\Omega^2 \tag{2.14}$$

Since there are two values of α and two values of β, the general solution has four arbitrary constants. It is convenient to use hyperbolic functions as the basis functions instead of exponential and write the general solution as

$$u=A\cosh\alpha y+B\cosh\beta y+C\sinh\alpha y+D\sinh\beta y \tag{2.15}$$

Then from Eqs. (2.12), we obtain the displacement v

$$v=-\mathrm{i}\frac{\alpha}{k}A\sinh\alpha y-\mathrm{i}\frac{k}{\beta}B\sinh\beta y-\mathrm{i}\frac{\alpha}{k}C\cosh\alpha y-\mathrm{i}\frac{k}{\beta}D\cosh\beta y \tag{2.16}$$

3. Solutions for symmetric loading

For the symmetric solutions, $C=D=0$. Now we take into account the free boundary conditions. It is convenient to redefine the other two constants by substituting $\mathrm{i}kA$ for A and $B\beta$ for B.

$$\begin{aligned} u&=\mathrm{i}kA\cosh\alpha y+B\beta\cosh\beta y\\ v&=\alpha A\sinh\alpha y-\mathrm{i}kB\sinh\beta y \end{aligned} \tag{3.1}$$

By substitution for these displacements in the stress equations (2.9) and using the definitions of the parameters α and β (2.14), we obtain

$$\begin{aligned}\sigma_{xx} &= A(\beta^2 - k^2 - 2\alpha^2)\cosh\alpha y + 2\beta B\mathrm{i}k\cosh\beta y\\ \sigma_{yy} &= A(k^2 + \beta^2)\cosh\alpha y - 2\beta B\mathrm{i}k\cosh\beta y\\ \sigma_{xy} &= 2\alpha A\mathrm{i}k\sinh\alpha y + (\beta^2 + k^2)B\sinh\beta y\end{aligned} \tag{3.2}$$

The free boundary conditions (2.3), using (3.2), yield two relations for the ratio of the constants A and B

$$\frac{A}{B} = \frac{2\beta\mathrm{i}k\cosh\beta}{\cosh\alpha(k^2+\beta^2)}, \quad \frac{A}{B} = \frac{\mathrm{i}(\beta^2+k^2)\sinh\beta}{2\alpha k\sinh\alpha} \tag{3.3}$$

The consistency of these equations, yields the dispersion equation

$$\frac{\tanh\beta}{\tanh\alpha} = \frac{4k^2\alpha\beta}{(k^2+\beta^2)^2} \tag{3.4}$$

Setting $B = 1$ and determining A from (3.3), we find the fundamental solution of the problem for each branch, as the related displacements and stresses

$$\begin{aligned}u(y,k) &= \frac{(\beta^2+k^2)\sinh\beta}{2\alpha\sinh\alpha}\cosh\alpha y + \beta\cosh\beta y\\ v(y,k) &= \frac{\mathrm{i}(\beta^2+k^2)\sinh\beta}{2k\sinh\alpha}\sinh\alpha y - \mathrm{i}k\sinh\beta y\\ \sigma_{xx}(y,k) &= \frac{\mathrm{i}(\beta^2+k^2)\sinh\beta}{2\alpha k\sinh\alpha}(\beta^2 - k^2 - 2\alpha^2)\cosh\alpha y + 2\beta\mathrm{i}k\cosh\beta y\\ \sigma_{yy}(y,k) &= \left(\frac{\cosh\beta\cosh\alpha y}{\cosh\alpha} - \cosh\beta y\right)2\beta\mathrm{i}k\\ \sigma_{xy}(y,k) &= \left(\frac{-\sinh\beta}{\sinh\alpha}\sinh\alpha y + \sinh\beta y\right)(\beta^2+k^2)\end{aligned} \tag{3.5}$$

The wave number k is a function of the frequency Ω, as determined from the dispersion equation (3.4). The first five branches of the dispersion equation (3.4) for small Ω are shown in Fig. 3. For consistency with

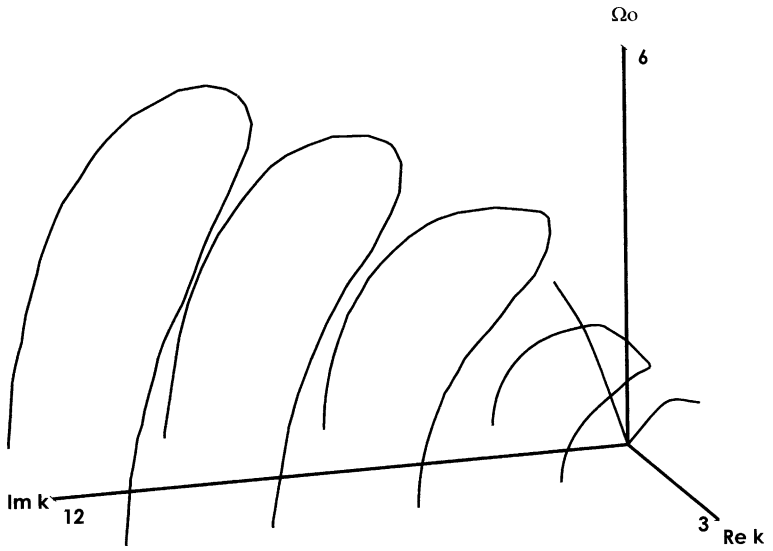

Fig. 3. Roots of dispersion equation vs. frequency, branches 0–4.

other authors, we plot the dimensionless frequency $\Omega_0^2 = (\rho h^2 \omega^2/(\lambda + 2\mu))$. The branches shown correspond to the non-growing solutions, related to $\mathrm{Im}\, k > 0$. There are also branches symmetric with respect to the plane $\mathrm{Re}\, k = 0$, obtained by replacing k by its negative conjugate $-\bar{k}$. We will number all the branches for small Ω, attaching index 0 to the penetrating branch and indices $1, 2, \ldots$ to branches with increasing $|k|$ for $\mathrm{Re}\, k > 0$, and indices $\bar{1}, \bar{2}, \ldots$ to the symmetric branches with $\mathrm{Re}\, k < 0$. For the ath branch, k_a is a function of Ω. According to (2.14), α and β area also functions of Ω. For definiteness when determining α and β from (2.14) as

$$\alpha = \sqrt{k^2 - \frac{1-2n}{2-2n} W^2}, \quad \beta = \sqrt{k^2 - \Omega^2}$$

we choose the branch of the square root $\sqrt{z}$ which obeys the rule $\alpha(\overline{-k}, \Omega) = \overline{\alpha(k, \Omega)}$, $\beta(-\bar{k}, \Omega) = \overline{\beta(k, \Omega)}$.

4. Series expansion

For the ath branch there are two real solutions, which are the real and imaginary parts (denoted by prime and double prime respectively) of the time dependent physical quantities. For the axial displacement, for example, these are denoted by $u'_a(x, y, t)$ and $u''_a(x, y, t)$. They are derived from the fundamental solution (3.5) and the equation

$$u(x, y, t, k_a) = u(y, k_a) \mathrm{e}^{\mathrm{i}(k_a x - \Omega t)} = u'_a(x, y, t) + \mathrm{i} u''_a(x, y, t) \tag{4.1}$$

Similarly

$$\begin{aligned}
v(x, y, t, k_a) &= v(y, k_a) \mathrm{e}^{\mathrm{i}(k_a x - \Omega t)} = v'_a(x, y, t) + \mathrm{i} v''_a(x, y, t) \\
\sigma_{xx}(x, y, t, k_a) &= \sigma_{xx}(y, k_a) \mathrm{e}^{\mathrm{i}(k_a x - \Omega t)} = \sigma'_{xx\ a}(x, y, t) + \mathrm{i}\sigma''_{xx\ a}(x, y, t) \\
\sigma_{yy}(x, y, t, k_a) &= \sigma_{yy}(y, k_a) \mathrm{e}^{\mathrm{i}(k_a x - \Omega t)} = \sigma'_{yy\ a}(x, y, t) + \mathrm{i}\sigma''_{yy\ a}(x, y, t) \\
\sigma_{xy}(x, y, t, k_a) &= \sigma_{xy}(y, k_a) \mathrm{e}^{\mathrm{i}(k_a x - \Omega t)} = \sigma'_{xy\ a}(x, y, t) + \mathrm{i}\sigma''_{xy\ a}(x, y, t)
\end{aligned}$$

From (4.1), the axial displacement components are:

$$\begin{aligned}
u'_a(x, y, t) &= (u'(y, k_a) \cos(k'_a x - \Omega t) - u''(y, k_a) \sin(k'_a x - \Omega t)) \mathrm{e}^{-k''_a x} \\
u''_a(x, y, t) &= (u'(y, k_a) \sin(k'_a x - \Omega t) + u''(y, k_a) \cos(k'_a x - \Omega t)) \mathrm{e}^{-k''_a x}
\end{aligned} \tag{4.2}$$

Similar formulas for the other physical quantities follow from (4.1). For the branches associated with the conjugate roots of the dispersion equation $-\bar{k}$, we have $u(\overline{-k}, \Omega) = \overline{u(k, \Omega)}$, $v(-\bar{k}, \Omega) = \overline{v(k, \Omega)}$ therefore

$$\begin{aligned}
u'_{\bar{a}}(x, y, t) &= (u'(y, k_a) \cos(k'_a x + \Omega t) - u''(y, k_a) \sin(k'_a x + \Omega t)) \mathrm{e}^{-k''_a x} \\
u''_{\bar{a}}(x, y, t) &= (-u'(y, k_a) \sin(k'_a x + \Omega t) - u''(y, k_a) \cos(k'_a x + \Omega t)) \mathrm{e}^{-k''_a x}
\end{aligned} \tag{4.3}$$

Again, similar formulas for the other physical quantities follow from (4.1) So, we have, for each branch with complex values for k, four independent real solutions. There are two penetrating branches with real wave numbers k and $-k$. They correspond to the waves running to the right and left respectively. We assume that here are no waves coming from infinity. Thus only one penetrating branch, that with positive k, should be taken into account. It generates two real independent solutions. It is easy to see that for small values of Ω, α is real while β is pure imaginary. Thus, for the penetrating branch

$$u'(y, k_0) = v''(y, k_0) = \sigma''_{xx}(y, k_0) = \sigma''_{yy}(y, k_0) = \sigma'_{xy}(y, k_0) = 0 \tag{4.4}$$

The two real independent solutions for the longitudinal displacements are

$$\begin{aligned} u'_0(x,y,t) &= -u''(y,k_0)\sin(k'_0x-\Omega t)\\ u''_0(x,y,t) &= u''(y,k_0)\cos(k'_0x-\Omega t) \end{aligned} \tag{4.5}$$

For each value of W, we may seek the solution of the boundary value problem in the form of series with respect to the obtained partial solutions. For example, for the axial component of displacements one can write

$$\begin{aligned} u(x,y,t) = &-A_0u''(y,k_0)\sin(k'_0x-\Omega t)+B_0u''(y,k_0)\cos(k'_0x-\Omega t)\\ &+\sum_{a=1}^{\infty}[A_au'_a(x,y,t)+B_au''_a(x,y,t)]+\sum_{\bar{a}=1}^{\infty}[C_au'_{\bar{a}}(x,y,t)+D_au''_{\bar{a}}(x,y,t)] \end{aligned} \tag{4.6}$$

At the edge $x=0$, using (4.2)–(4.5), this becomes

$$\begin{aligned} u(0,y,t) = &A_0u''_{xx}(y,k_0)\sin\Omega t+B_0u''_{xx}(y,k_0)\cos\Omega t+\sum_{a=1}^{\infty}[(A_a+C_a)u'_{xx}(y,k_a)+(B_a-D_a)u''_{xx}(y,k_a)]\cos\Omega t\\ &+\sum_{a=1}^{\infty}[(A_a-C_a)u''_{xx}(y,k_a)-(B_a+D_a)u'_{xx}(y,k_a)]\sin\Omega t \end{aligned} \tag{4.7}$$

Similar formulas and expansions hold for the other fields.

The coefficients A_0, B_0, A_a, B_a, C_a, D_a should be found from the boundary conditions (2.4) and (2.5). Let us write down these conditions explicitly in terms of the unknown coefficients.

$$\begin{aligned} &A_0\sigma'_{xx}(y,k_0)+\sum_{a=1}^{\infty}(A_a+C_a)\sigma'_{xx}(y,k_a)+(B_a-D_a)(\sigma''_{xx}(y,k_a))=f_{xx}(y)\\ &-B_0\sigma'_{xx}(y,k_0)+\sum_{a=1}^{\infty}-(B_a+D_a)\sigma'_{xx}(y,k_a)+(A_a-C_a)\sigma''_{xx}(y,k_a)=g_{xx}(y)\\ &B_0\sigma''_{xy}(y,k_0)+\sum_{a=1}^{\infty}(A_a+C_a)\sigma'_{xy}(y,k_a)+(B_a-D_a)\sigma''_{xy}(y,k_a)=f_{xy}(y)\\ &A_0\sigma''_{xy}(y,k_0)+\sum_{a=1}^{\infty}-(B_a+D_a)\sigma'_{xy}(y,k_a)+(A_a-C_a)\sigma''_{xy}(y,k_a)=g_{xy}(y) \end{aligned} \tag{4.8}$$

The penetrating stress for the given applied load may be computed from (4.8) by determining the coefficients A_0 and B_0. The basic functions in this expansion, $\sigma'_{xx}(y,k_a)$, $\sigma''_{xx}(y,k_a)$, $\sigma'_{xy}(y,k_a)$ and $\sigma''_{xy}(y,k_a)$ look, to some extent, similar to the basic functions of a Fourier series. They are shown for each of the first five branches, normalized by the maximum amplitude of the real part of the axial stress in each branch, in Fig. 4–7, for a frequency $\Omega_0=0.3$. At this frequency, the associated values of k are

Branch	Re k	Im k
0	0.319	0
1	1.129	2.058
2	1.553	5.359
3	1.776	8.526
4	1.930	11.691

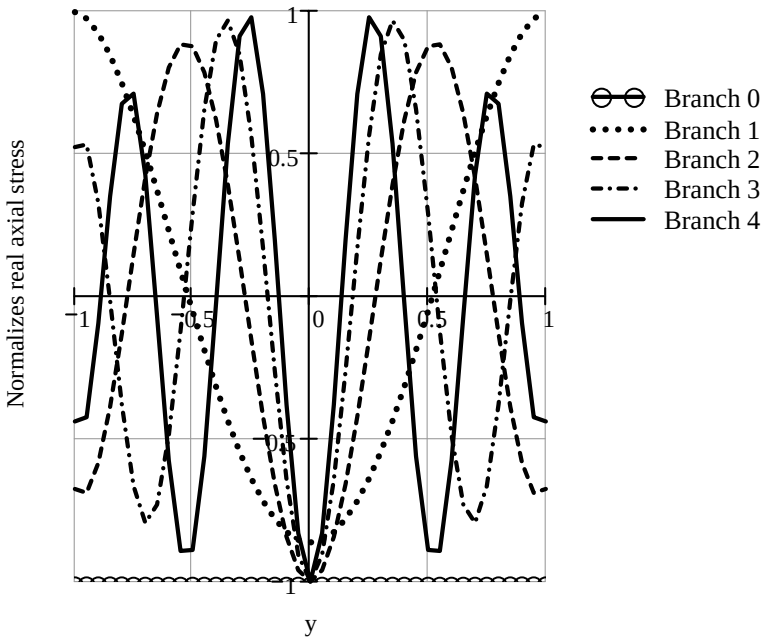

Fig. 4. Real part of the axial stress Eq. (3.5) vs. distance across strip for the first five symmetric branches, normalized by the amplitude of the maximum axial stress.

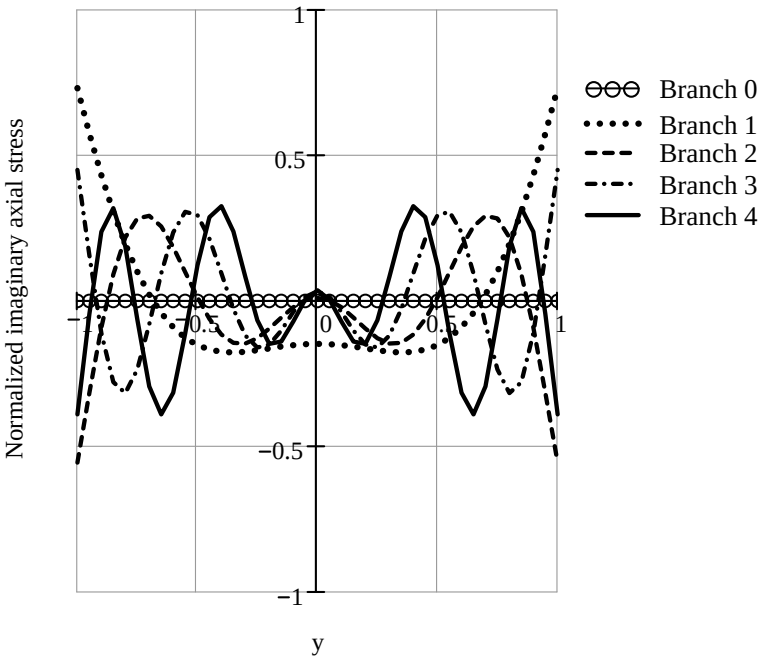

Fig. 5. Imaginary part of the axial stress Eq. (3.5) vs. distance across strip for the first five symmetric branches, normalized by the amplitude of the maximum axial stress.

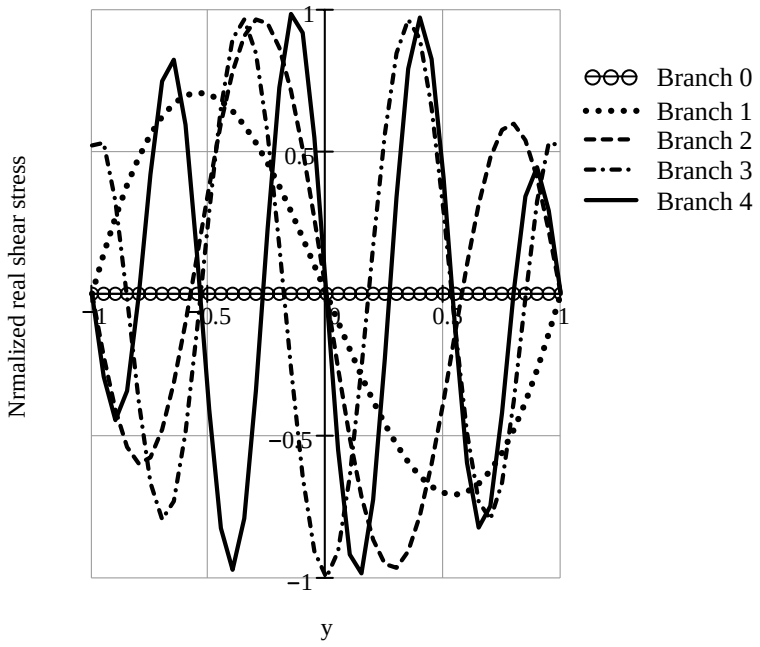

Fig. 6. Real part of the shear stress Eq. (3.5) vs. distance across strip for the first five symmetric branches, normalized by the amplitude of the maximum axial stress.

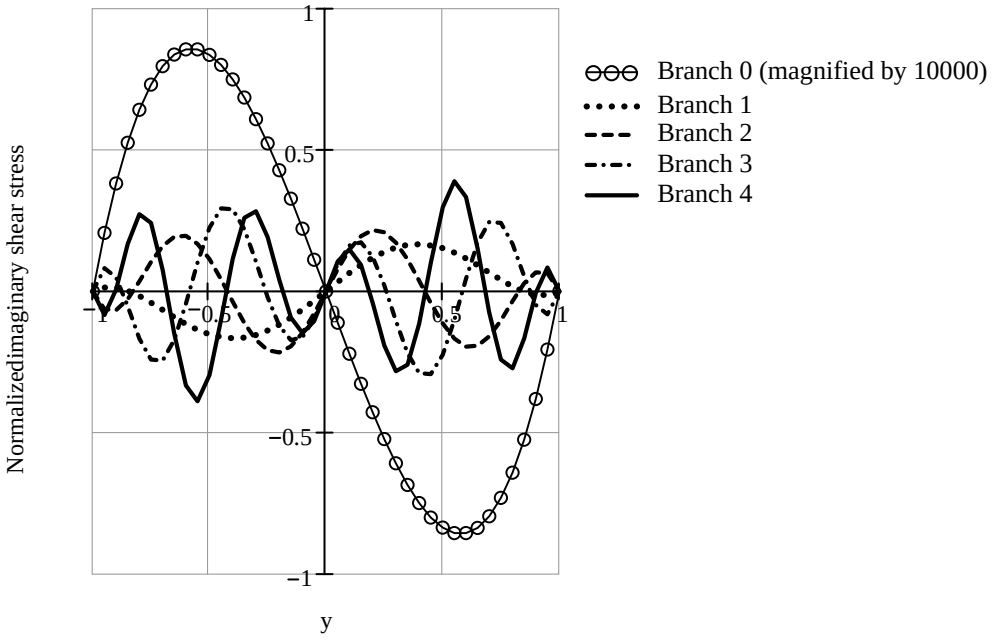

Fig. 7. Imaginary part of the shear stress Eq. (3.5) vs. distance across strip for the first five symmetric branches, normalized by the amplitude of the maximum axial stress.

5. Probabilistic model and results for symmetric loading

We intend to find from the system of Eqs. (4.8) the coefficients A_0, B_0 which specify the magnitude of the penetrating stress state. We assume that the load is self-equilibrated. Due to the symmetry properties of the problem for a self-equilibrated load, functions $f_{xx}(y)$ and $g_{xx}(y)$ must obey the conditions

$$\int_{-1}^{1} f_{xx}(y)\,\mathrm{d}y = \int_{-1}^{1} g_{xx}(y)\,\mathrm{d}y = 0 \tag{5.1}$$

while functions $f_{xy}(y)$, $g_{xy}(y)$ inherently satisfy the self-equilibrated load condition. If nothing is known about the self-equilibrated load, then nothing can be said about the penetrating stress state. We are going to provide probabilistic information about the self-equilibrated load and seek the probabilistic characteristics of the penetrating stress state. The problem can be considerably simplified if we note that there should be a one-to-one correspondence between the coefficients A_0, B_0, A_a, B_a, C_a, D_a and the functions $f_{xx}(y)$, $f_{xy}(y)$, $g_{xx}(y)$ and $g_{xy}(y)$. The two conditions (5.1) serve to specify the values of A_0 and B_0.

Absence of knowledge of $f_{xx}(y)$, $f_{xy}(y)$, $g_{xx}(y)$ and $g_{xy}(y)$ corresponds to the absence of knowledge of the coefficients A_a, B_a, C_a and D_a. Therefore, instead of prescribing a probabilistic model for $f_{xx}(y)$, $f_{xy}(y)$, $g_{xx}(y)$ and $g_{xy}(y)$, one can give a probabilistic model for the coefficients A_a, B_a, C_a and D_a. We assume in what follows that these coefficients are independent Gaussian random variables with zero mean and unit variances. Then the coefficients A_0 and B_0 determined from (5.1) as linear functions of A_a, B_a, C_a and D_a are also Gaussian variables with zero mean, at least if we keep in the series a finite number of terms.

The degree to which Saint-Venant's principle is violated may be characterized by the ratio θ of the maximum penetrating stress to the maximum value of the stress at the loaded end.

$$\theta = \frac{\sqrt{A_0^2 + B_0^2}\,\max_y \sqrt{\sigma'_{xx}(y,k_0)^2 + 2\sigma''_{xy}(y,k_0)^2 + \sigma'_{yy}(y,k_0)^2}}{\max_y \sqrt{f_{xx}(y)^2 + g_{xx}(y)^2 + 2f_{xy}(y)^2 + 2g_{xy}(y)^2 + f_{yy}(y)^2 + g_{yy}(y)^2}} \tag{5.2}$$

where $f_{yy}(y)\cos\Omega t + g_{yy}(y)\sin\Omega t$ is the yy-component of the stress tensor at $x = 0$. If the self-equilibrated load at the beam end is of the same order as the non-equilibrated one then θ may serve as a measure of the error induced by using Saint-Venant's principle in dynamical problems. Ratio θ is a random variable. Its properties were determined numerically by running a Monte-Carlo analysis, where for each of 250 calculation the coefficients A_a, B_a, C_a and D_a were randomly selected from a set of Gaussian variables with zero mean and variance of unity. One may expect that, for each frequency, θ is bounded and has some maximum value. Therefore the beta distribution may be tried to smooth the histogram of the numerical results. For a random variable whose values lie between zero and one, the beta distribution has a probability density $p(x)$ given by

$$p(x) = \left\{ \begin{array}{ll} \dfrac{1}{B(a,b)} x^{a-1}(1-x)^{b-1} & 0 < x \leqslant 1 \\ 0 & \text{otherwise} \end{array} \right\} \tag{5.3}$$

where the constant $B(a,b)$ which normalizes the distribution can be expressed in terms of the Γ-function, as

$$B(a,b) = \int_0^1 x^{a-1}(1-x)^{b-1}\,\mathrm{d}x = \frac{\Gamma(a)\Gamma(b)}{\Gamma(a+b)} \tag{5.4}$$

For a random variable with the set of possible values in some finite interval $[0,d]$ the beta distribution should be scaled accordingly. The mean value of the variable x on the segment $[0,d]$ is

$$\bar{x}' = d\frac{a}{a+b} \tag{5.5}$$

The beta distribution approximation for the probability density of θ for two values of frequency is shown in Fig. 8 as the solid lines. The computed values for the parameters a and b were nearly constant across all frequencies with $\Omega_0 \leqslant 1.2$, with $a = 2.4$ and $b = 3.8$. The increase in the average value $\bar{\theta}$ as frequency increases correlates with increase in the parameter d.

The average value $\bar{\theta}$ as a function of frequency is depicted in Fig. 9, solid line. We see from Fig. 9 that Saint-Venant's principle produces average errors less than 7% if frequency $\Omega_0 \leqslant 1.2$. Note that this is an

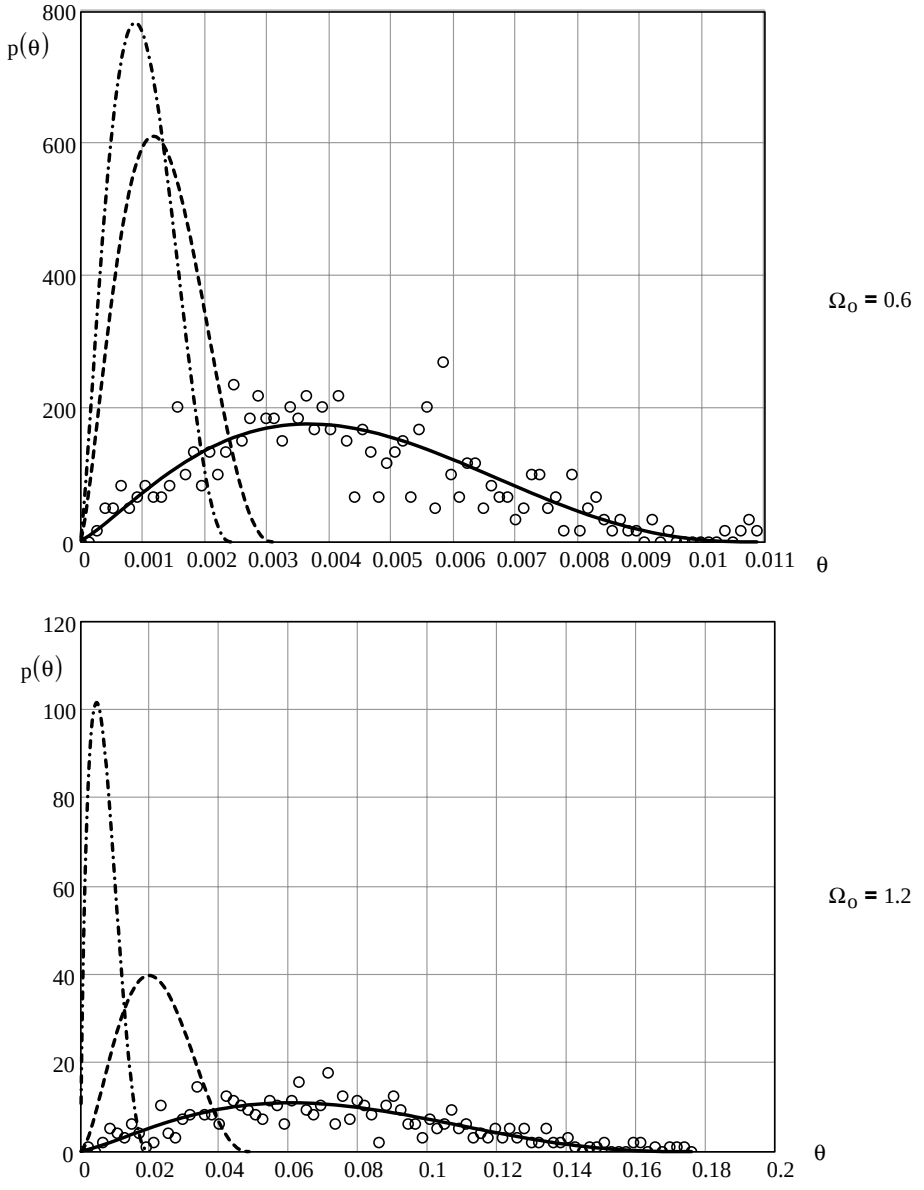

Fig. 8. Probability density function for the ratio of maximum penetrating stress to maximum end stress at two frequencies, in classical theory (solid line with raw data dots) refined theory with boundary conditions (5.6) (dashed line) refined theory with boundary conditions (5.7) (dash-dot line).

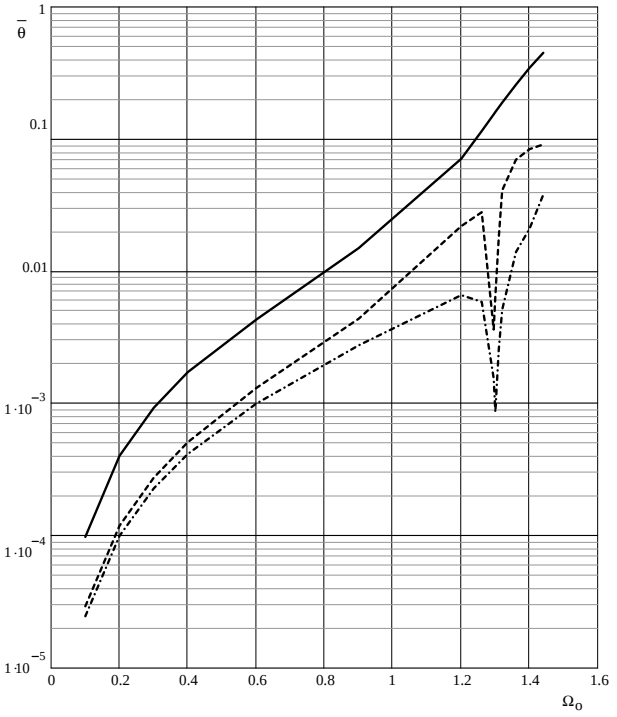

Fig. 9. Mean value of the ratio of maximum penetrating stress to maximum end stress vs. frequency in classical theory (solid line) refined theory with boundary conditions (5.6) (dashed line) refined theory with boundary conditions (5.7) (dash-dot line).

average estimate: in fact, errors may be bigger than 7% for a particular load, as follows from the probability distributions shown in Fig. 8.

Integrating the probability density function $p(\theta)$ up to a certain given value Θ, one determines the probability $P(\Theta)$ that error is less than Θ. Subtracting this value from unity gives the probability $Q(\Theta) = 1 - P(\Theta)$ that the error exceeds the certain value Θ. A graph of $Q(\Theta)$ is given in Fig. 10 for the frequencies $\Omega_0 = 0.6$ and $\Omega_0 = 1.2$. From these graphs we see that the probability of the error being greater than 10% (i.e. $\Theta \geqslant 0.1$) was 0.2 for a frequency $\Omega_0 = 1.2$ but the probability of the error being greater than 1% is near zero for $\Omega_0 = 0.6$.

The situation improves in the refined one-dimensional beam theories where a larger number of the end conditions must be satisfied. For example, the theory by Berdichevsky and Le (1980) requires that, in addition to the usual self-equilibrating condition $\int_{-1}^{1} \sigma_{xx}\,\mathrm{d}y = 0$, the stresses must also obey the conditions

$$\int_{-1}^{1} \sigma_{xx} \cos \pi y\,\mathrm{d}y = 0 \quad \text{and} \quad \int_{-1}^{1} \sigma_{xy} \sin \frac{\pi y}{2}\,\mathrm{d}y = 0. \tag{5.6}$$

Thus, in the Berdichevsky–Le theory we have, in addition to (5.1), the constraints:

$$\int_{-1}^{1} f_{xx} \cos \pi y\,\mathrm{d}y = \int_{-1}^{1} g_{xx} \cos \pi y\,\mathrm{d}y = \int_{-1}^{1} f_{xy} \sin \frac{\pi}{2} y\,\mathrm{d}y = \int_{-1}^{1} g_{xy} \sin \frac{\pi}{2} y\,\mathrm{d}y = 0$$

They are satisfied by determining the coefficients A_1, B_1, C_1, D_1 of the series expansion in addition to A_0, B_0. Undetermined coefficients are assumed as before, statistically independent Gaussian random variables with zero mean and unit variance. The average values of $\bar{\theta}$ vs. frequency is shown in Fig. 9, dash line. The dent in

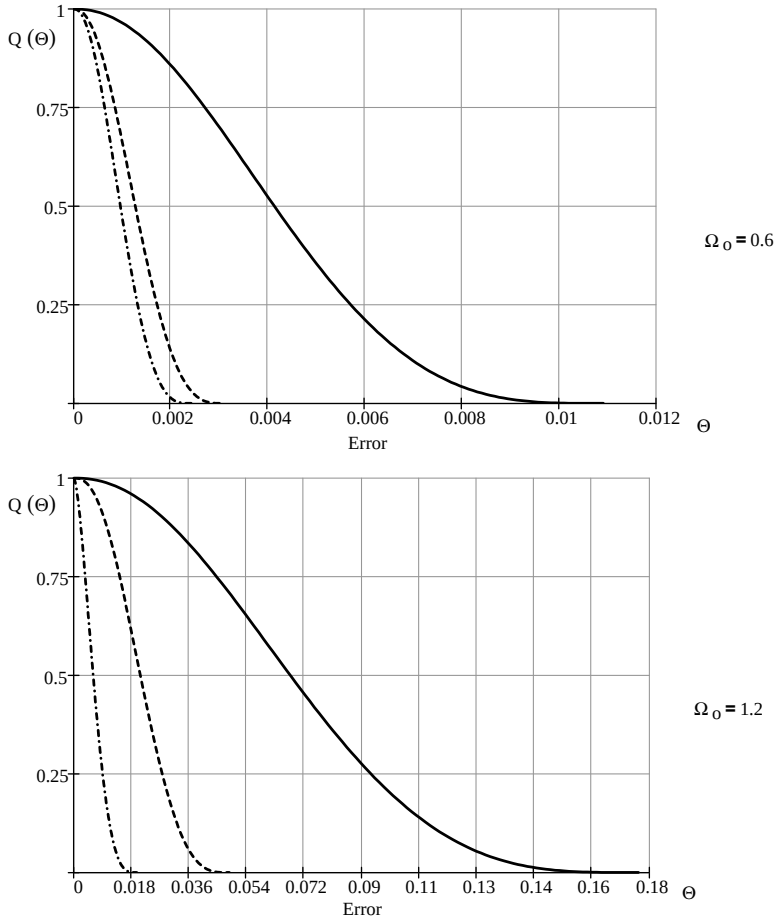

Fig. 10. Probability $Q(\Theta)$ that the ratio exceeds the value Θ at two frequencies classical theory (solid line) refined theory with boundary conditions (5.6) (dashed line) refined theory with boundary conditions (5.7) (dash-dot line).

the curve corresponds to the edge resonance effect which occurs at a frequency $\Omega_0 = 1.3$. This resonance is also documented by Gregory and Gladwell (1983). The average error does not exceed 9% anywhere in the frequency range considered, $\Omega_0 \leqslant 1.44$. The probability distribution of θ for the Berdichevsky–Le theory is shown in Fig. 8, dash line. The computed values for the parameters a and b were again nearly constant across all frequencies where $\Omega_0 \leqslant 1.2$, with $a = 2.4$ and $b = 3.8$. As the frequency approached that of the edge resonance effect, both the parameters a and b showed a rapid increase, reaching a value of 15 at $\Omega_0 = 1.3$, then decreasing at the same rate as the frequency increased to $\Omega_0 = 1.44$. From Fig. 10, dash line, we see that the error will be less than 5% for a frequency $W_0 = 1.2$ and less than 0.3% at a frequency $\Omega_0 = 0.6$.

Interestingly, a change of the weighting factor, so that the shear stress constraint condition $\int_{-1}^{1} \sigma_{xy} \sin(\pi y/2)\,\mathrm{d}y = 0$ is replaced by $\int_{-1}^{1} \sigma_{xy} \sin \pi y\,\mathrm{d}y = 0$ reduces the error further, as shown by the dash-dot lines in Figs. 8–10. The reason is that the weighting factor $\sin(\pi y/2)$ came from consideration of the first high frequency branch, while we here consider the frequency range where the lateral stress is approximated well by $\sin \pi y$.

In the numerical simulation which produced the quoted results, five modes from the entire series were used. Further analysis showed that the presence of the higher harmonics of the self-equilibrated load

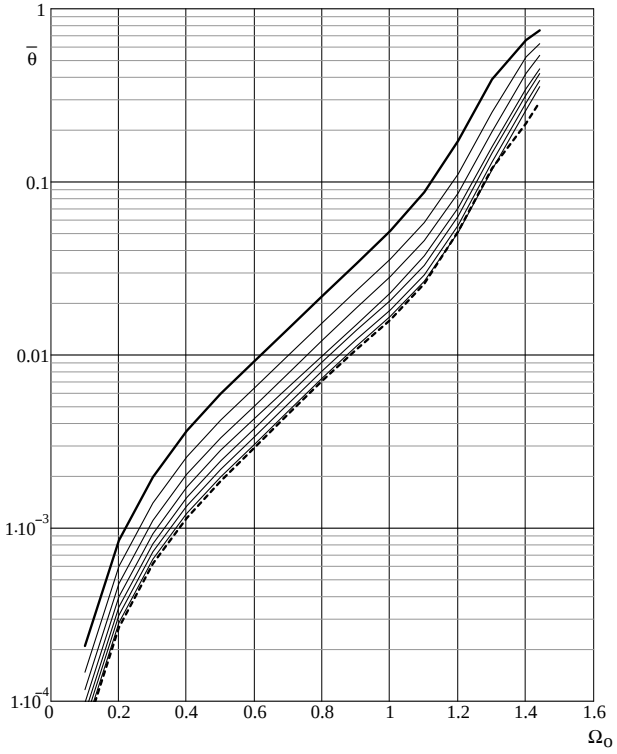

Fig. 11. Average ratio of the maximum penetrating stress to the maximum applied stress vs. frequency for classical theory with just 2 branches involved (heavy solid line) with 3–8 branches involved (fainter lines) and an extrapolation to an infinite number of branches (heavy dash line).

distribution which are associated with higher mode numbers caused a reduction of the ratios θ. To obtain information on the effect of the number of branches, computations of the ratio for the case of A_a, B_a, C_a and D_a being Gaussian variables with zero mean and unit variance, for $1 \leqslant a \leqslant 7$ (i.e from 2 to 8 branches including the propagating branch) showed that the ratio seems converging with increase in number of branches considered. The results of the calculations and an exponentially fitted extrapolation to an infinite number of branches is given in Fig. 11. From this, it is concluded that a smooth self-equilibrated load will cause a larger ratio of propagated to applied stress than a highly irregular one, by about a factor of four.

The effect on the results of the sample size to be included in a Monte-Carlo analysis was studied, where the number of branches involved were five. The estimated ratio of maximum propagated to maximum applied stress was determined at four frequencies $\Omega_0 = 0.6$, 1.1, 1.2 and 1.3. The values for the ratio when 50 samples were used were about 10% lower than when more than 150 samples were included. There was less than 1% variation in the estimated ratio when 150, 250, 350 or 450 samples were included.

6. Conclusion

We have proposed an approach to describe quantitatively the violation of Saint-Venant's principle in dynamic problems. We used this approach to determine the probability that the error of classical engineering theory exceeds certain levels for longitudinal vibrations of a two-dimensional semi-infinite strip. We

quantify also the improvement achieved by the use of a refined engineering beam theory. For a dimensionless frequency $\Omega_0 = 0.6$ the error of classical theory was less than 1%, with overwhelming probability. For frequency $\Omega_0 = 1.2$ the probability of error to be 5% was considerable, about 0.7, the probability of the error to be 10% was about 0.2, while the probability that the error exceeded 15% was negligible. Use of the refined theory resulted in an error certainly less than 5% for $\Omega_0 \leqslant 1.2$. The numerical results were found to depend on the measure used to represent the applied load. A more irregular applied load resulted in a smaller error incurred from the use of engineering beam theory.

References

Baxter, S.C., Horgan, C.O., 1997. Anti-plane shear deformations of anisotropic sandwich structures; end effects. International Journal of Solids and Structures 34 (1), 79–98.

Berdichevsky, V., 1974. On the proof of the Saint-Venant principle for bodies of arbitrary shape. Journal of Applied Mathematics and Mechanics (PMM) 38 (5).

Berdichevsky, V., 1976. Damping rate of stresses in cylindrical elastic bodies. Soviet Physics A Doklady 21 (9), 534–536.

Berdichevsky, V., 1978. Energy methods in some problems of decay of solutions. Journal of Applied Mathematics and Mechanics (PMM) 42 (1), 140–156.

Berdichevsky, V., Le, K.C., 1980. High frequency, long wave shell vibration. Journal of Applied Mathematics and Mechanics (PMM) 44, 520–525.

Berdichevsky, V., 1981. On the energy of an elastic rod. Journal of Applied Mathematics and Mechanics (PMM) 45 (4), 518–529.

De Saint-Venant, B., 1885. Memoir sur la torsion des prismes. MemDivers Savants 1.

Druz, A.N., Ustinov, Y.A., 1996. Green's tensor for an elastic cylinder and its applications in the development of the Saint-Venant theory. Journal of Applied Mathematics and Mechanics (PMM) 60 (1), 97–104.

Flavin, J.N., Knops, R.J., 1987. Some spatial decay estimates in continuum mechanics. Journal of Elasticity 17, 249–264.

Flavin, J.N., Knops, R.J., 1988. Some decay and other estimates in two-dimensional linear elasticity. Quarterly Journal of Mechanics and Applied Mathematics 41 (2), 223–238.

Flavin, J.N., Knops, R.J., Payne, I.E., 1989. Decay estimates for the constrained elastic cylinder of variable cross-section. Quarterly Applied Mathematics 47, 323–350.

Flavin, J.N., Rionero, S., 1993. Decay and other estimates for an elastic cylinder. Quarterly Journal of Mechanics and Applied Mathematics 46, 299–309.

Folk, R., Herczynski, A., 1986. Solutions of elastodynamic slab problems using a new orthogonality condition. Journal of Acoustical Society of America 80 (4), 1103–1110.

Gregory, R.D., Gladwell, J., 1983. The reflection of a symmetric Rayleigh–Lamb wave at the fixed or free edge of a plate. Journal of Elasticity 13, 185–206.

Horgan, C.O., 1974. The axisymmetric end problem for transversely isotropic circular cylinders. International Journal of Solids and Structures 10, 837–852.

Horgan, C.O., Knowles, J.K., 1983. Recent developments concerning Saint-Venant's principle. In: Wu, T.Y., Hutchinson, J.W. (Eds.), Advances in Applied Mechanics, vol. 23. pp. 179–269.

Horgan, C.O., 1989. Recent developments concerning Saint-Venant's principle; an update. Applied Mechanics Reviews 42, 295–303.

Horgan, C.O., 1996. Recent developments concerning Saint-Venant's principle; a second update. Applied Mechanics Reviews 49 (10), 101–111.

Knowles, J.K., 1966. On Saint-Venant's principle in the two-dimensional theory of elasticity. Archives for Rational Mechanics and Analysis 21, 1–22.

Knowles, J.K., Horgan, C.O., 1969. On the exponential decay of stress in circular elastic cylinders subject to axisymmetric self-equilibrating end loads. International Journal of Solids and Structures 5, 33–50.

Lamb, H., 1916. On waves in an elastic plate. Proceedings of the Royal Society of London Series A 93, 114–128.

Le, K.C., 1999. Vibrations of shells and rods. ISBN 3-540-64516-0. Springer-Verlag, Berlin, Heidelberg, New York.

Mason, W.P. (Ed.), 1964. Physical Acoustics: Principles and Methods, vol. 10. Academic Press, New York, p. 18.

Matemilola, S.A., Stronge, W.J., 1995. Diffusion rate for stress in orthotropic materials. Journal of Applied Mechanics—Transactions of ASME 62 (3), 654–661.

Meleshko, V.V., Tatuyan, V.B., 1987. Generation of harmonic Lamb waves in a semi-infinite elastic layer. Soviet Physics Acoustics 35 (5), 532–536.

Mielke, A., 1989. Normal hyperelasticity of center manifolds and Saint-Venant's principle. Archives for Rational Mechanics and Analysis 110 (4), 353–372.

Mindlin, R.D., Medick, M.A., 1959. Extensional vibrations of elastic plates. Journal of Applied Mechanics—Transactions of ASME 26, 561–569.

Novozhilov, V.V., Slepian, L.I., 1964. On Saint-Venant's principle in the dynamics of beams. Journal of Applied Mathematics and Mechanics (PMM) 29 (2), 261–281.

Pagneux, V., Maurel, A., 2001. Determination of Lamb mode eigenvalues. Journal of Acoustical Society of America 110 (3), 1307–1314.

Rassoulova, N.B., 2001. On dynamics of bar of rectangular cross section. Journal of Applied Mechanics—Transactions of the ASME 68, 662–666.

Toupin, R.A., 1965. Saint-Venant's principle. Archives for Rational Mechanics and Analysis 18, 83–96.

Tullini, N., Horgan, C.O., 1998. End effects for anti-plane shear deformations of periodically laminated strips with imperfect bonding. Journal of Elasticity 50 (3), 227–244.

Vafeades, P., Horgan, C.O., 1988. Exponential decay estimates for solutions to the Von-Karman equations on a semi-infinite strip. Archives for Rational Mechanics and Analysis 104 (1), 1–25.

Volovoi, V., Hodges, D., Berdichevsky, V., Sutyrin, V., 1998. Dynamic dispersion curves for non-homogeneous anisotropic beams with cross sections of arbitrary geometry. Journal of Sound and Vibration 115 (5), 1101–1120.

Volovoi, V., Hodges, D., Berdichevsky, V., Sutyrin, V., 1999. Asymptotic theory for static behavior of elastic anisotropic I-beams. International Journal of Solids and Structures 36 (7), 1017–1043.

Wijeyewickrema, A.C., Horgan, C.O., Dundurs, J., 1996. Further analysis of end effects for plane deformations of sandwich strips. International Journal of Solids and Structures 33 (29), 4327–4336.